ARTICLES

Diphthamide biosynthesis requires an organic radical generated by an iron–sulphur enzyme

Yang Zhang[1]*, Xuling Zhu[1]*, Andrew T. Torelli[1], Michael Lee[2], Boris Dzikovski[1], Rachel M. Koralewski[1], Eileen Wang[1], Jack Freed[1], Carsten Krebs[2,3], Steven E. Ealick[1] & Hening Lin[1]

Archaeal and eukaryotic translation elongation factor 2 contain a unique post-translationally modified histidine residue called diphthamide, which is the target of diphtheria toxin. The biosynthesis of diphthamide was proposed to involve three steps, with the first being the formation of a C–C bond between the histidine residue and the 3-amino-3-carboxypropyl group of *S*-adenosyl-L-methionine (SAM). However, further details of the biosynthesis remain unknown. Here we present structural and biochemical evidence showing that the first step of diphthamide biosynthesis in the archaeon *Pyrococcus horikoshii* uses a novel iron–sulphur-cluster enzyme, Dph2. Dph2 is a homodimer and each of its monomers contains a [4Fe–4S] cluster. Biochemical data suggest that unlike the enzymes in the radical SAM superfamily, Dph2 does not form the canonical 5′-deoxyadenosyl radical. Instead, it breaks the $C_{\gamma,Met}$–S bond of SAM and generates a 3-amino-3-carboxylpropyl radical. Our results suggest that *P. horikoshii* Dph2 represents a previously unknown, SAM-dependent, [4Fe–4S]-containing enzyme that catalyses unprecedented chemistry.

Corynebacterium diphtheriae is a pathogenic bacterium that causes the infectious disease diphtheria in humans[1]. This bacterium kills host cells by secreting a protein factor, diphtheria toxin[2], that catalyses the ADP-ribosylation of a post-translationally modified histidine residue (Fig. 1) in eukaryotic translation elongation factor 2 (eEF2)[3]. Because this post-translational modification is the target of diphtheria toxin, it was named diphthamide. eEF2 is a GTPase required for the translocation step of ribosomal protein synthesis[4]. The diphthamide modification is conserved in all eukaryotes and archaea and is important for ribosomal protein synthesis[4,5]. Although diphthamide was identified more than three decades ago, its biosynthesis has remained an enigma[6]. Five genes required for diphthamide biosynthesis, *DPH1*, *DPH2*, *DPH3*, *DPH4* and *DPH5*[3,7–13] (yeast nomenclature), have been identified in eukaryotes, and a biosynthetic pathway has been proposed (Fig. 1).

The first step of diphthamide biosynthesis, the transfer of the 3-amino-3-carboxypropyl (ACP) group from SAM to the C2 position of the imidazole ring of the target histidine residue in eEF2, is catalysed by Dph1–4 in eukaryotes. This step is followed by a trimethylation, catalysed by Dph5, and an amidation, catalysed by an unidentified enzyme. The first step is particularly interesting for several reasons. First, SAM is generally a methyl donor, but in the

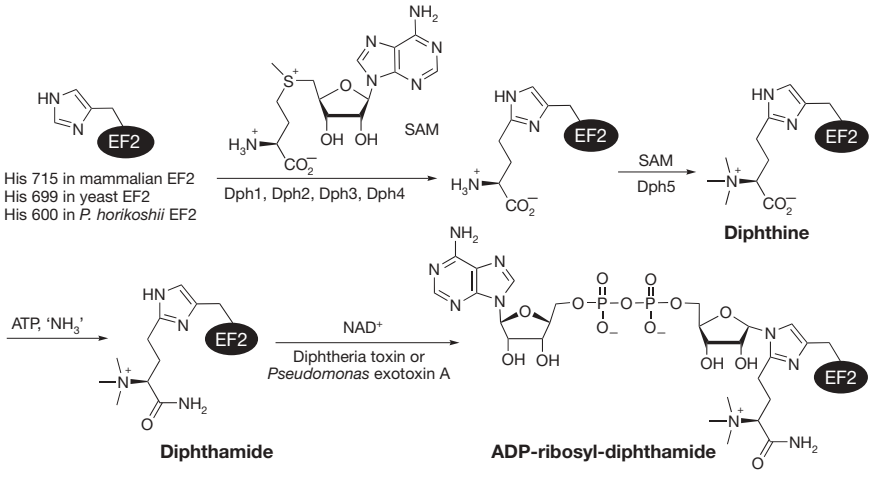

Figure 1 | The structure of diphthamide and its proposed biosynthesis pathway. The diphthamide residue is the target of bacterial ADP-ribosyltransferases, diphtheria toxin and *Pseudomonas* exotoxin A. EF2, translation elongation factor 2.

[1]Department of Chemistry and Chemical Biology, Cornell University, Ithaca, New York 14853, USA. [2]Department of Biochemistry and Molecular Biology, The Pennsylvania State University, University Park, Pennsylvania 16802, USA. [3]Department of Chemistry, The Pennsylvania State University, University Park, Pennsylvania 16802, USA.
*These authors contributed equally to this work.

first step the ACP group is transferred from SAM. Second, protein post-translational modifications that involve the formation of C–C bonds are rare[6] and in diphthamide biosynthesis this formation involves the poorly nucleophilic C2 of the imidazole ring. Third, in eukaryotes this reaction requires four proteins, Dph1–4, raising questions about the function of each protein.

Eukaryotic Dph1 and Dph2 share about 20% sequence identity, but are not similar to any other protein with known function. Iterative BLAST searches[14] starting with *Saccharomyces cerevisiae* Dph1 or Dph2 generate both proteins from other eukaryotic species. In contrast, BLAST searches identify only one protein, Dph2, in archaeal species. Archaeal Dph2 proteins are more similar to eukaryotic Dph1 than to Dph2. Eukaryotic Dph3 and Dph4 have no orthologues in archaea on the basis of BLAST searches. To better understand diphthamide biosynthesis, we initially attempted to reconstitute the first step using *P. horikoshii* Dph2 (PhDph2) and translation elongation factor 2 (PhEF2) under aerobic conditions without success. The X-ray crystal structure of PhDph2 revealed an intriguing constellation of three conserved cysteine residues—each from a different structural domain—suggestive of an iron–sulphur cluster. Subsequently, PhDph2 activity was reconstituted in the presence of dithionite under anaerobic conditions. A crystal structure of reconstituted PhDph2 along with ultraviolet–visible, electron paramagnetic resonance (EPR) and Mössbauer spectroscopy confirmed the presence of a [4Fe–4S] cluster. Detailed biochemical characterization suggests that the PhDph2-catalysed reaction involves an ACP radical intermediate. The data suggest that PhDph2 is a novel, SAM-dependent, [4Fe–4S]-containing enzyme[15] that catalyses unprecedented chemistry.

PhDph2 is aerobically inactive

PhDph2 and PhEF2 were expressed in *Escherichia coli* and purified under aerobic conditions. No activity was observed when using these proteins to reconstitute the first step of diphthamide biosynthesis. One explanation for the lack of activity is that the reaction requires an oxygen-sensitive cofactor and another is that additional proteins or small molecules are required. In the second case, the additional proteins might be orthologues of eukaryotic Dph3 and Dph4; however, attempts to reconstitute activity under similar conditions using yeast Dph1–4 and eEF2 were also unsuccessful (data not shown).

Crystal structure of PhDph2

To provide structural insight into the catalytic mechanism of PhDph2, we determined its X-ray crystal structure at 2.3 Å resolution using selenomethionine (SeMet) single-wavelength anomalous diffraction phasing. The structure showed that PhDph2 is a homodimer (Fig. 2). Each PhDph2 monomer consists of three domains, all sharing the same overall fold. The basic domain fold is a four-stranded parallel β-sheet with three flanking α-helices (or two α-helices and one 3_{10} helix in the case of domain 2) (Supplementary Fig. 1). The two β-sheets in domains 1 and 2 each contain an additional β-strand that is antiparallel to the rest of the β-sheet. Domains 2 and 3 have two additional α-helices. Domain 1 of one monomer and domain 3 of the adjacent monomer form the dimer interface, creating an extended, nine-stranded β-sheet. The domain folds and their arrangement resemble the structure of quinolinate synthase[16]; however, the orientations of the domains with respect to each other are different in the two enzymes (Supplementary Fig. 2). Three conserved cysteine residues (Cys 59, Cys 163 and Cys 287), each coming from a different structural domain, are clustered together in the centre of the PhDph2 monomers. All three cysteine residues are conserved in eukaryotic Dph1. The first and third cysteine residues are conserved in eukaryotic Dph2 (Supplementary Fig. 3).

Reconstitution of PhDph2 activity

The clustering of the three cysteine residues in the crystal structure and the requirement for SAM raised the possibility that PhDph2 uses a [4Fe–4S] cluster[15]. Radical SAM enzymes harbour a [4Fe–4S] cluster coordinated by three cysteines in a CX_3CX_2C motif[17] (although variations of this motif have been reported[18,19]) to generate a 5′-deoxyadenosyl radical. Because [4Fe–4S] clusters are typically oxygen sensitive, we purified and assayed PhDph2 anaerobically. Using ^{14}C-SAM, we showed that PhEF2 can be labelled in the presence of PhDph2 (Fig. 3a, lane 6), but not in the absence of PhDph2 (lane 3) or dithionite (lane 7). When His 600 of PhEF2, the site of the diphthamide modification, was changed to alanine, no reaction occurred in the presence of PhDph2 (lane 5). Matrix-assisted laser desorption/ionization mass spectrometry of the PhEF2 protein confirmed that an ACP group was added after the reaction (Fig. 3b). These results suggest the possibility that PhDph2 is a SAM-dependent iron–sulphur enzyme and demonstrate that no other enzyme is required for the first step of diphthamide biosynthesis *in vitro*.

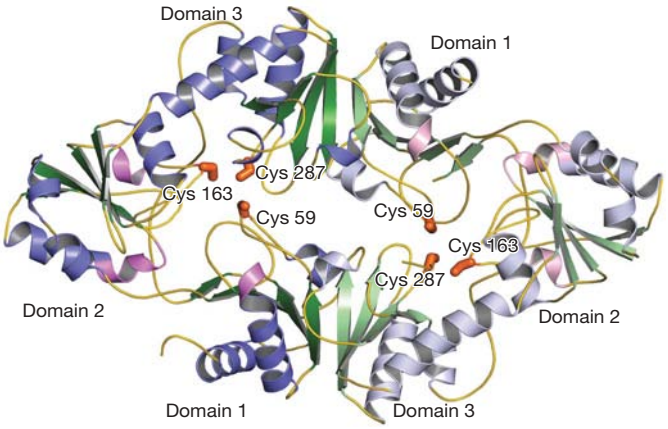

Figure 2 | Structure of the PhDPH2 homodimer. Ribbon diagram of the PhDph2 homodimer with one monomer in dark colours and the other in light colours. Each monomer is also coloured according to secondary structure, with dark and light green for β-strands, dark and light blue for α-helices and violet and pink for 3_{10} helices. The three conserved cysteine residues for each monomer are shown in the stick representation, in orange.

Characterization of the [4Fe–4S] cluster

The anaerobically purified PhDph2 contains 1.3 ± 0.2 and 1.9 ± 0.2 equiv. of iron and, respectively, sulphur per polypeptide, and displays a broad absorption band, at ~400 nm, that disappears on reduction by 0.5 mM dithionite (Fig. 4a). The 400-nm absorption is typical of a $[4Fe–4S]^{2+}$ cluster. Quantification based on the 400-nm absorption suggests the presence of ~0.3 $[4Fe–4S]^{2+}$ clusters per PhDph2. EPR spectra of dithionite-reduced PhDph2 are shown in Fig. 4b. The *g* values (2.03, 1.92 and 1.86) and the temperature dependence are typical of a $[4Fe–4S]^{+}$ cluster[20–23]. Quantification of the EPR spectrum also suggests the presence of ~0.3 $[4Fe–4S]^{+}$ clusters per PhDph2.

The ^{57}Fe-enriched, anaerobically isolated PhDph2 contains 2.0 ± 0.2 and 2.1 ± 0.2 equiv. of iron and sulphur per polypeptide, respectively. The 4.2-K/53-mT Mössbauer spectrum (Fig. 4c) is dominated (73% of total intensity) by a quadrupole doublet with parameters typical of $[4Fe–4S]^{2+}$ clusters (an isomer shift (δ) of $0.43\ mm\ s^{-1}$ (see Methods for standard used) and a quadrupole splitting parameter (ΔE_Q) of $1.13\ mm\ s^{-1}$; Fig. 4c, solid line). The weak absorption peak labelled (a) suggests the presence of a small amount (~10%) of high-spin Fe(II), which is presumably non-specifically bound to the protein. The shoulder labelled (b) belongs to a quadrupole doublet (~15% intensity), the left line of which contributes to the prominent peak at $-0.2\ mm\ s^{-1}$. Although the nature of the iron species that gives rise to this absorption is not known, similar spectral features were observed for a sample of *P. horikoshii* quinolinate synthase[24], which is structurally similar to PhDph2 and also harbours a [4Fe–4S] cluster. Thus, all the spectroscopic data indicate that PhDph2 contains a [4Fe–4S] cluster.

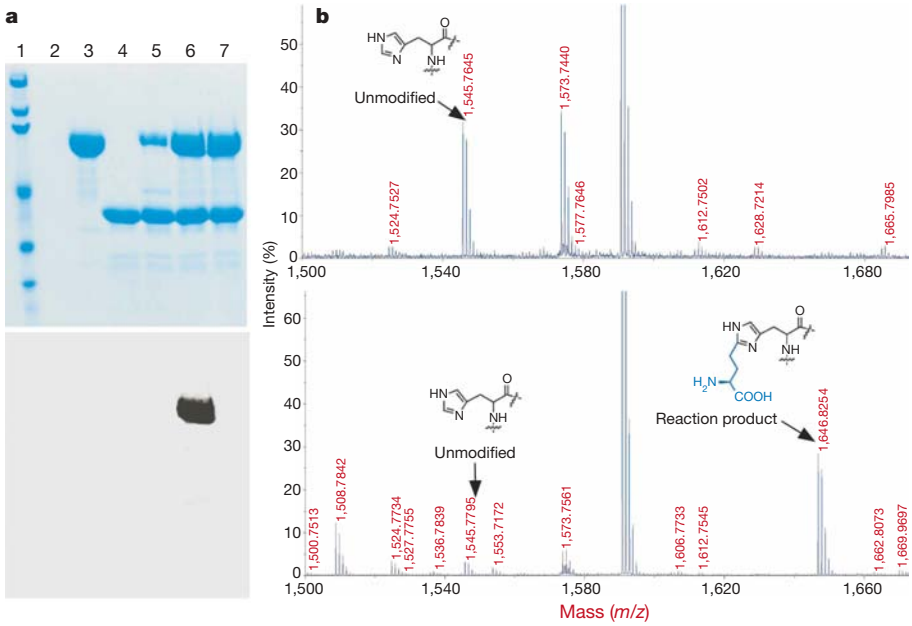

Figure 3 | *In vitro* reconstitution of PhDph2 activity. **a**, Activity assay using carboxy-^{14}C-SAM: the top panel shows the Coomassie-blue-stained gel; the bottom panel shows the autoradiography. Lane 1: protein standard; lane 2: blank lane; lane 3: PhEF2 plus SAM, negative control; lane 4: PhDph2 plus SAM, negative control; lane 5: PhEF2 His600Ala plus PhDph2 plus SAM, negative control; lane 6: PhEF2 plus PhDph2 plus SAM plus dithionite; lane 7: PhEF2 plus PhDph2 plus SAM, no dithionite, negative control. **b**, The matrix-assisted laser desorption/ionization mass spectra of PhEF2 unmodified (top) and modified by PhDph2 in an *in vitro* reaction (bottom).

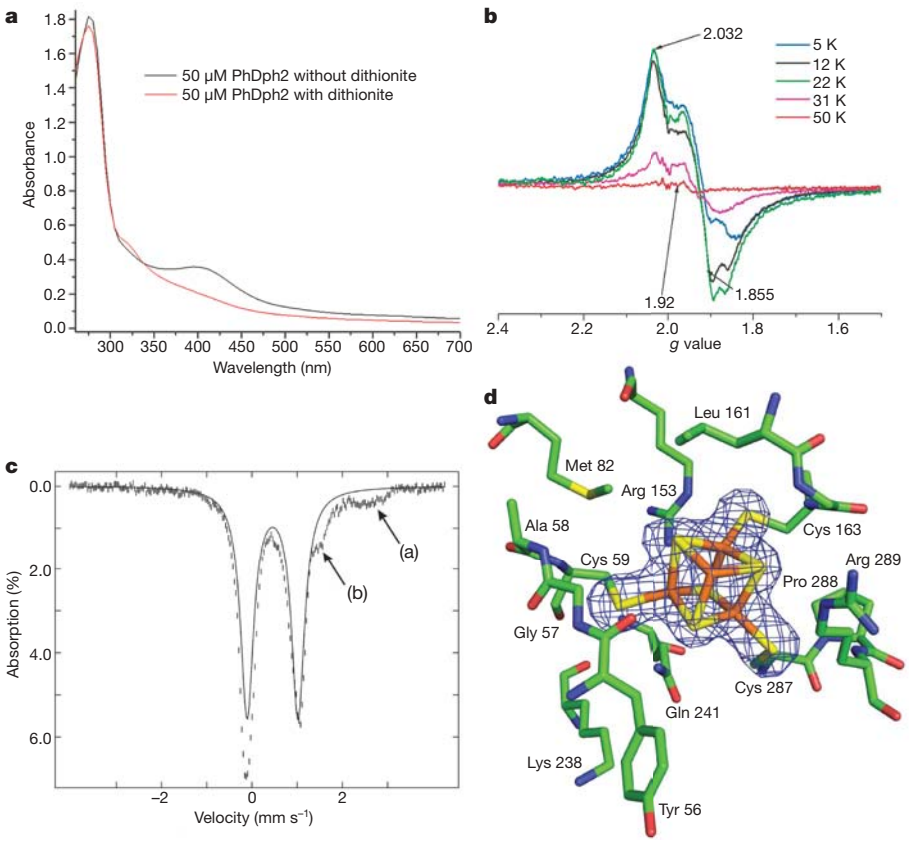

Figure 4 | Spectroscopic characterization of the [4Fe–4S] cluster in PhDph2. **a**, Ultraviolet–visible absorption spectra of anaerobically isolated and dithionite-reduced PhDph2. **b**, X-band EPR spectra of dithionite-reduced PhDph2 at different temperatures. **c**, 4.2-K/53-mT Mössbauer spectrum of anaerobically isolated, ^{57}Fe-labelled PhDph2 expressed in *E. coli*. The horizontal axis shows the velocity of the γ-ray source. **d**, Structure of PhDph2 including the [4Fe–4S] cluster. C, green; O, red; N, blue; S, yellow; Fe, orange.

Brown crystals of the anaerobically purified PhDph2 were obtained that belong to the same space group as the inactive PhDph2. A crystal structure determined to 2.1 Å resolution showed clear electron density for a [4Fe–4S] cluster (Fig. 4d and Supplementary Fig. 4). Refinement of the PhDph2 structure with a [4Fe–4S] cluster included gave final R and R_{free} values of 20.4% and 25.2%, respectively (Supplementary Table 1).

Reaction mechanism

To explore the PhDph2 reaction mechanism, we used high-performance liquid chromatography to analyse the reaction products. In the reaction that contained SAM, PhDph2, PhEF2 and dithionite, most SAM molecules were converted to 5′-deoxy-5′-methylthioadenosine (MTA; Fig. 5a). In control reactions without PhDph2 or dithionite, only low concentrations of MTA were observed and most SAM molecules were left intact. This is consistent with the activity assay results shown in Fig. 3. Cleavage of the C5′–S bond of SAM did not occur because the formation of 5′-deoxyadenosine (the most likely product of the adenosyl moiety) was not observed. Collectively, the results suggest that PhDph2 catalyses the cleavage of the $C_{\gamma,Met}$–S bond of SAM only in the presence of reductant, transfers the ACP group to PhEF2 and releases the remaining MTA.

Two different mechanisms can be proposed for the PhDph2-catalysed cleavage of the $C_{\gamma,Met}$–S bond of SAM. One is that the $[4Fe–4S]^{+}$ cluster provides one electron to reductively cleave the $C_{\gamma,Met}$–S bond of SAM, forming MTA, an ACP radical and the oxidized $[4Fe–4S]^{2+}$ cluster (Supplementary Fig. 5a). Alternatively, the [4Fe–4S] cluster in PhDph2 binds SAM and orients it correctly for nucleophilic attack by the C2 of the imidazole ring (Supplementary Fig. 5b), leading to the formation of products. Further evidence to differentiate these two possibilities was provided by the identification of the product derived from the ACP group in the reaction without PhEF2. In the absence of PhEF2, PhDph2 can still cleave the $C_{\gamma,Met}$–S bond of SAM, generating MTA (Fig. 5a). We investigated the fate of the ACP group using ^{1}H NMR (Fig. 5b). In the reaction containing PhDph2, SAM and dithionite, we observed several new peaks that were not seen in control samples without dithionite or PhDph2 (Fig. 5b). These peaks were assigned to two products: 2-aminobutyric acid (ABA) and homocysteine sulphinic acid (HSA). The NMR spectra of authentic samples of ABA and HSA confirmed these assignments (Fig. 5b). In Supplementary Fig. 6, these NMR spectra are compared with those of homoserine, homoserine lactone and SAM, ruling out the possibility that PhDph2 catalyses the formation of homoserine or homoserine lactone by means of a nucleophilic mechanism.

To further validate these results, the reaction mixtures were purified by thin-layer chromatography, dansylated and subsequently analysed by liquid chromatography/mass spectroscopy (LC–MS). The structures and molecular weights of the dansylated compounds

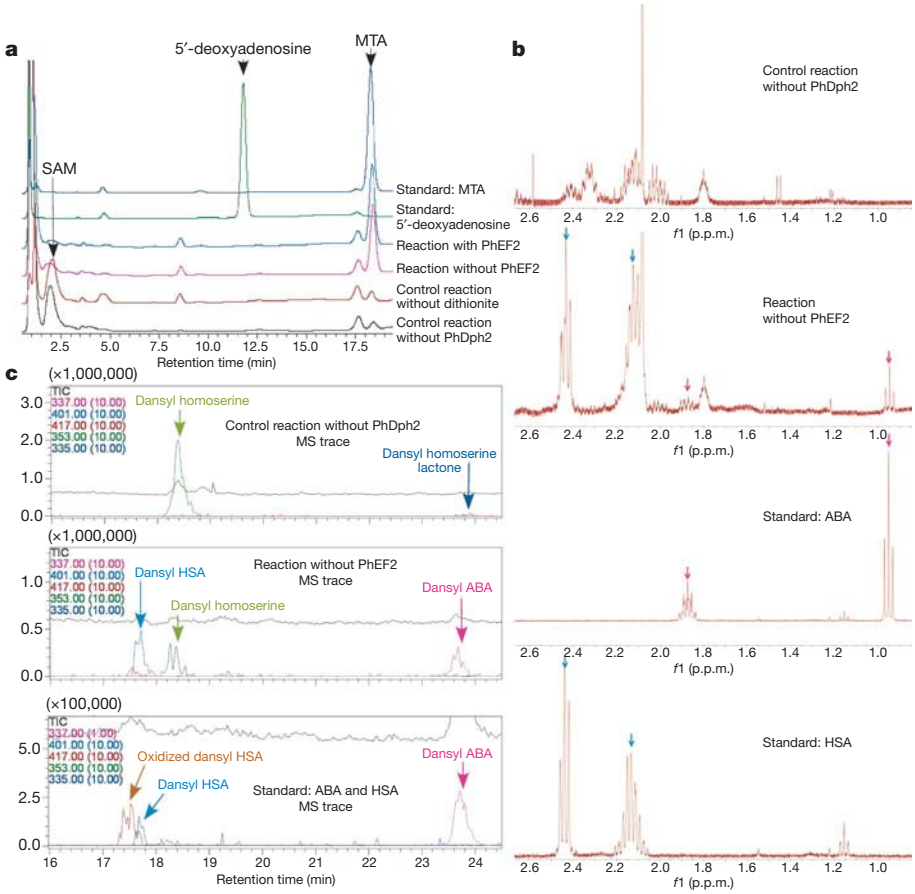

Figure 5 | Identification of SAM-derived small-molecule products in PhDph2-catalysed reactions. **a**, High-performance liquid chromatography analysis of reaction products suggests that PhDph2 does not form 5′-deoxyadenosine. **b**, ^{1}H NMR spectra showing that ABA and HSA formed in the reaction when PhEF2 was not present, but not in a control reaction in which PhDph2 was not present. The peaks from HSA and ABA are marked by blue and magenta arrows, respectively. $f1$, chemical shift in the F1 dimension. **c**, Detection of dansylated reaction products by LC–MS. The mass spectroscopy (MS) traces (total ion counts (TIC) and ion counts for specific compounds) are shown for the reaction with PhDph2, the control reaction without PhDph2, and ABA and HSA standards. TIC is indicated by the axis value times the magnification number, either 1,000,000 or 100,000, whereas the specific ion counts are magnified by a factor of ten from their actual values. The m/z value for each specific ion is indicated in the upper left corner, and followed by the magnification number. For example, in the upper panel, the specific ion for dansyl homoserine, m/z 353 (green), has ion count ~2,000,000 and its actual value is 200,000.

are shown in Supplementary Fig. 7. In the control reaction without PhDPh2, the formation of dansylated homoserine (m/z 337, MH^+, retention time 18.35 min) was observed (Fig. 5c and Supplementary Fig. 8), which is consistent with the NMR results (Supplementary Fig. 6). In the reaction with PhDph2, SAM and dithionite, the formation of dansylated homoserine was suppressed in comparison with the control. Instead, dansylated ABA (m/z 337, MH^+, 23.60 min) and HSA (m/z 401, MH^+, 16.65 min) were observed (Fig. 5c and Supplementary Fig. 8). Dansylated homoserine lactone and ABA have the same retention time, but can be differentiated by their m/z values (337 and 335 for ABA and homoserine lactone, respectively; Supplementary Fig. 9). During the thin-layer chromatography purification and dansylation reaction, HSA was partly oxidized to homocysteine sulphonic acid, as evidenced by the ion with m/z 417 (MH^+; Fig. 5c and Supplementary Fig. 8). Overall, the results from the LC–MS and NMR analyses demonstrate that PhDph2 catalyses the formation of ABA and HAS in the absence of PhEF2. The formation of ABA and HSA can be best explained by the generation of an ACP radical followed by hydrogen abstraction to give ABA or quenching by dithionite to give HSA (Fig. 6).

Discussion

The biochemical, structural and spectroscopic data presented here establish that PhDph2 is a novel [4Fe–4S]-cluster enzyme. PhDph2 cleaves the $C_{\gamma,Met}$–S bond of SAM to MTA and transfers the ACP group to His 600 of PhEF2. This reaction is strictly dependent on the presence of reductant. In the absence of the natural substrate, PhEF2, the ACP moiety is trapped either as ABA or as HSA, which suggests the intermediacy of an ACP radical. The reductive cleavage of SAM to a thioether and an alkyl radical by a reduced $[4Fe–4S]^+$ cluster is the hallmark of the superfamily of radical SAM enzymes[15]. However, there are two crucial differences between the radical SAM enzymes and PhDph2. First, the radical SAM enzymes exclusively cleave the C5′–S bond to generate methionine and a 5′-deoxyadenosyl radical, which is used for a variety of downstream C–H cleavage reactions. Second, the radical SAM superfamily is characterized by a conserved CX_3CX_2C motif[17] (CX_2CX_4C in ThiC[18] and CX_5CX_2C in HmdA[19]) that binds the [4Fe–4S] cluster. This motif is not present in PhDph2. Instead, the three conserved cysteine residues are located in separate structural domains and are separated by more than 100 residues in the sequence. Consequently, the three-dimensional structure of PhDph2 is distinct from the structures of the known radical SAM enzymes BioB[25], HemN[26], lysine-2,3-aminomutase[27], MoaA[28], pyruvate–formate-lyase-activating enzyme[29] and ThiC[18], which all have β-barrel or modified β-barrel folds. PhDph2 is structurally similar to quinolinate synthase[16], which is also composed of three structurally homologous domains in a triangular arrangement. The triangular arrangement of domains in PhDph2 positions the three conserved cysteine residues in the central cavity to bind the [4Fe–4S] cluster. In quinolinate synthase, the three conserved cysteine residues required to bind the cluster are also widely separated in the amino-acid sequence and are located in different domains[23,30]. However, quinolinate synthase is not SAM dependent and its proposed role is in the dehydration of the penultimate precursor of quinolinate[23]. In addition, the IspH enzyme in the non-mevalonate pathway for isoprenoid biosynthesis also uses a similar triangular arrangement to bind a [3Fe–4S] cluster[31].

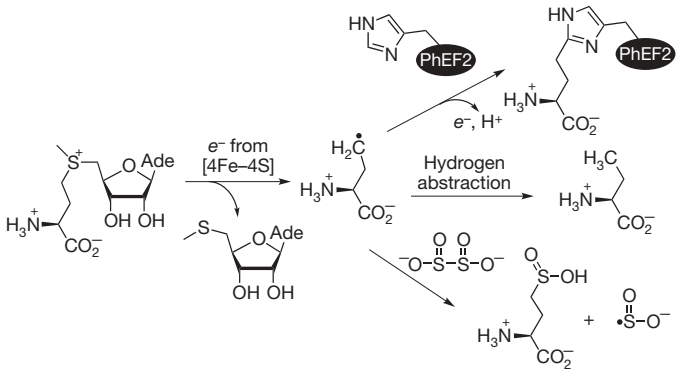

Figure 6 | The proposed reaction mechanism for PhDph2. The formation of ABA and HSA can be best explained by an ACP radical intermediate. The radical can be generated by electron transfer from the [4Fe–4S] cluster, similar to the generation of a 5′-deoxyadenosyl radical in other radical SAM enzymes. In the presence of PhEF2, the radical will react with PhEF2 to form the modified PhEF2 product. In the absence of PhEF2, the radical can either abstract a hydrogen atom to form ABA or be quenched by dithionite to give HSA. Ade, adenosine base.

It is likely that the different reaction outcome, that is, cleavage of the C5′–S bond in the radical SAM enzymes versus cleavage of the $C_{\gamma,Met}$–S bond in PhDph2, is controlled by SAM having different orientations relative to the [4Fe–4S] cluster. In the radical SAM enzymes, the amino and carboxyl groups of SAM coordinate to the non-cysteine-ligated iron site of the [4Fe–4S] cluster[32]. Future structural and spectroscopic studies are required to investigate how SAM is bound at the active site of PhDph2.

Our data demonstrate that PhDph2 is the only gene product required to catalyse the first step of diphthamide biosynthesis *in vitro*. In contrast, biosynthesis of diphthamide in eukaryotes requires four gene products, Dph1–4. Studies on PhDph2 provide important insight into the functions of eukaryotic Dph1–4. The crystal structure shows that PhDph2 is a homodimer. Eukaryotic Dph1 and Dph2 are homologous to each other and to archaeal Dph2. In addition, Dph1 and Dph2 in eukaryotes form a heterodimer[3,33–35]. Therefore, it is possible that the eukaryotic Dph1–Dph2 heterodimer is structurally homologous to the PhDph2 homodimer. The three cysteine residues required to bind the cluster are conserved in Dph1 and two of the cysteine residues are conserved in Dph2. Thus, the heterodimer of Dph1–Dph2 should at least bind one [4Fe–4S] cluster and may be sufficient to catalyse the first step *in vitro*. Dph2, which has only two of the conserved cysteine residues, could either have a different catalytic function from Dph1 or be regulatory. *In vivo*, Dph3 and Dph4 are also required for diphthamide biosynthesis[3]. These gene products may be required to keep the [4Fe–4S] cluster in a reduced state. This hypothesis is supported by the observation that Dph3 can bind iron and is redox active[36]. Alternatively, Dph3 and Dph4 may be required for proper assembly of the [4Fe–4S] clusters. The iron–sulphur-cluster assembly pathways in bacteria and the mitochondria of eukaryotes are known to involve J-domain-containing co-chaperone proteins, such as bacterial HscB and yeast Jac1[37,38], that are similar to Dph4. Confirmation of these functional assignments awaits detailed biochemical and structural studies.

METHODS SUMMARY

Crystallization, data collection and structure determination. We crystallized SeMet PhDph2 and anaerobically reconstituted PhDph2 using the hanging-drop vapour-diffusion method. The X-ray data were collected at the NE-CAT beamlines at the Advanced Photon Source, Argonne National Laboratory. The structures of iron-free PhDph2 and reconstituted PhDph2 were determined by SeMet single-wavelength anomalous diffraction phasing and Fourier synthesis, respectively.

Reconstitution of activity. Reconstituted PhDph2 was prepared by growing cells in lysogeny broth medium supplemented with $FeCl_3$, $Fe(NH_4)_2(SO_4)_2$ and L-cysteine, and purified using Ni-NTA affinity chromatography anaerobically. We monitored the reaction using carboxyl-^{14}C-SAM.

Analysis of reaction products. The formation of MTA was detected using high-performance liquid chromatography. Modification of PhEF2 His 600 was confirmed by matrix-assisted laser desorption/ionization mass spectrometry after trypsin digestion. The products derived from the ACP group were detected by NMR directly and by LC–MS after dansylation.

EPR and Mössbauer spectroscopy. We recorded EPR spectra on a Bruker EMX spectrometer at a frequency of 9.24 GHz under standard conditions. Mössbauer spectra were recorded on a spectrometer from WEB Research operating in the constant-acceleration mode in transmission geometry.

Full Methods and any associated references are available in the online version of the paper at www.nature.com/nature.

Received 6 December 2009; accepted 30 April 2010.
Published online XX 2010.

1. Centers for Disease Control and Prevention. Diphtheria. *Disease Listing, Diphtheria, Technical Information | CDC Bacterial, Mycotic Diseases* ⟨http://www.cdc.gov/ncidod/DBMD/diseaseinfo/diptheria_t.htm⟩ (2005).
2. Collier, R. J. Understanding the mode of action of diphtheria toxin: a perspective on progress during the 20th century. *Toxicon* **39,** 1793–1803 (2001).
3. Liu, S., Milne, G. T., Kuremsky, J. G., Fink, G. R. & Leppla, S. H. Identification of the proteins required for biosynthesis of diphthamide, the target of bacterial ADP-ribosylating toxins on translation elongation factor 2. *Mol. Cell. Biol.* **24,** 9487–9497 (2004).
4. Gomez-Lorenzo, M. G. *et al.* Three-dimensional cryo-electron microscopy localization of EF2 in the *Saccharomyces cerevisiae* 80S ribosome at 17.5 Å resolution. *EMBO J.* **19,** 2710–2718 (2000).
5. Ortiz, P. A., Ulloque, R., Kihara, G. K., Zheng, H. & Kinzy, T. G. Translation elongation factor 2 anticodon mimicry domain mutants affect fidelity and diphtheria toxin resistance. *J. Biol. Chem.* **281,** 32639–32648 (2006).
6. Walsh, C. T. *Posttranslational Modifications of Proteins: Expanding Nature's Inventory* 321–323 (Roberts, 2006).
7. Moehring, J. M., Moehring, T. J. & Danley, D. E. Posttranslational modification of elongation factor 2 in diphtheriatoxin-resistant mutants of CHO-K1 cells. *Proc. Natl Acad. Sci. USA* **77,** 1010–1014 (1980).
8. Moehring, T. J., Danley, D. E. & Moehring, J. M. *In vitro* biosynthesis of diphthamide, studied with mutant Chinese hamster ovary cells resistant to diphtheria toxin. *Mol. Cell. Biol.* **4,** 642–650 (1984).
9. Chen, J. Y., Bodley, J. W. & Livingston, D. M. Diphtheria toxin-resistant mutants of *Saccharomyces cerevisiae. Mol. Cell. Biol.* **5,** 3357–3360 (1985).
10. Mattheakis, L. C., Shen, W. H. & Collier, R. J. *DPH5,* a methyltransferase gene required for diphthamide biosynthesis in *Saccharomyces cerevisiae. Mol. Cell. Biol.* **12,** 4026–4037 (1992).
11. Mattheakis, L. C., Sor, F. & Collier, R. J. Diphthamide synthesis in *Saccharomyces cerevisiae*: structure of the *DPH2* gene. *Gene* **132,** 149–154 (1993).
12. Phillips, N. J., Ziegler, M. R. & Deaven, L. L. A cDNA from the ovarian cancer critical region of deletion on chromosome 17p13.3. *Cancer Lett.* **102,** 85–90 (1996).
13. Schultz, D. C., Balasara, B. R., Testa, J. R. & Godwin, A. K. Cloning and localization of a human diphthamide biosynthesis-like protein-2 gene, *DPH2L2*. *Genomics* **52,** 186–191 (1998).
14. Altschul, S. F., Gish, W., Miller, W., Myers, E. W. & Lipman, D. J. Basic local alignment search tool. *J. Mol. Biol.* **215,** 403–410 (1990).
15. Frey, P. A., Hegeman, A. D. & Ruzicka, F. J. The radical SAM superfamily. *Crit. Rev. Biochem. Mol. Biol.* **43,** 63–88 (2008).
16. Sakuraba, H., Tsuge, H., Yoneda, K., Katunuma, N. & Ohshima, T. Crystal structure of the NAD biosynthetic enzyme quinolinate synthase. *J. Biol. Chem.* **280,** 26645–26648 (2005).
17. Sofia, H. J., Chen, G., Hetzler, B. G., Reyes-Spindola, J. F. & Miller, N. E. Radical SAM, a novel protein superfamily linking unresolved steps in familiar biosynthetic pathways with radical mechanisms: functional characterization using new analysis and information visualization methods. *Nucleic Acids Res.* **29,** 1097–1106 (2001).
18. Chatterjee, A. *et al.* Reconstitution of ThiC in thiamine pyrimidine biosynthesis expands the radical SAM superfamily. *Nature Chem. Biol.* **4,** 758–765 (2008).
19. McGlynn, S. E. *et al.* Identification and characterization of a novel member of the radical AdoMet enzyme superfamily and implications for the biosynthesis of the Hmd hydrogenase active site cofactor. *J. Bacteriol.* **192,** 595–598 (2010).
20. Makinen, G. B. & Wells, M. W. in *ENDOR, EPR and Electron Spin Echo for Probing Coordination Spheres* (eds Sigel, H. & Sigel, A.) 129–204 (Dekker, 1987).
21. Lieder, K. W. *et al. S*-adenosylmethionine-dependent reduction of lysine 2,3-aminomutase and observation of the catalytically functional iron–sulfur centers by electron paramagnetic resonance. *Biochemistry* **37,** 2578–2585 (1998).
22. Walsby, C. J. *et al.* Electron-nuclear double resonance spectroscopic evidence that *S*-adenosylmethionine binds in contact with the catalytically active $[4Fe–4S]^{+}$ cluster of pyruvate formate-lyase activating enzyme. *J. Am. Chem. Soc.* **124,** 3143–3151 (2002).
23. Cicchillo, R. M. *et al. Escherichia coli* quinolinate synthetase does indeed harbor a [4Fe-4S] cluster. *J. Am. Chem. Soc.* **127,** 7310–7311 (2005).
24. Saunders, A. H. *et al.* Characterization of quinolinate synthases from *Escherichia coli, Mycobacterium tuberculosis*, and *Pyrococcus horikoshii* indicates that [4Fe-4S] clusters are common cofactors throughout this class of enzymes. *Biochemistry* **47,** 10999–11012 (2008).
25. Berkovitch, F., Nicolet, Y., Wan, J. T., Jarrett, J. T. & Drennan, C. L. Crystal structure of biotin synthase, an *S*-adenosylmethionine-dependent radical enzyme. *Science* **303,** 76–79 (2004).
26. Layer, G., Moser, J., Heinz, D. W., Jahn, D. & Schubert, W.-D. Crystal structure of coproporphyrinogen III oxidase reveals cofactor geometry of radical SAM enzymes. *EMBO J.* **22,** 6214–6224 (2003).
27. Lepore, B. W., Ruzicka, F. J., Frey, P. A. & Ringe, D. The X-ray crystal structure of lysine-2,3-aminomutase from *Clostridium subterminale. Proc. Natl Acad. Sci. USA* **102,** 13819–13824 (2005).
28. Hänzelmann, P. & Schindelin, H. Crystal structure of the *S*-adenosylmethionine-dependent enzyme MoaA and its implications for molybdenum cofactor deficiency in humans. *Proc. Natl Acad. Sci. USA* **101,** 12870–12875 (2004).
29. Vey, J. L. *et al.* Structural basis for glycyl radical formation by pyruvate formate-lyase activating enzyme. *Proc. Natl Acad. Sci. USA* **105,** 16137–16141 (2008).
30. Marinoni, I. *et al.* Characterization of L-aspartate oxidase and quinolinate synthase from *Bacillus subtilis. FEBS J.* **275,** 5090–5107 (2008).
31. Rekittke, I. *et al.* Structure of (*E*)-4-hydroxy-3-methyl-but-2-enyl diphosphate reductase, the terminal enzyme of the non-mevalonate pathway. *J. Am. Chem. Soc.* **130,** 17206–17207 (2008).
32. Walsby, C. J., Ortillo, D., Broderick, W. E., Broderick, J. B. & Hoffman, B. M. An anchoring role for FeS clusters: chelation of the amino acid moiety of S-adenosylmethionine to the unique iron site of the [4Fe–4S] cluster of pyruvate formate-lyase activating enzyme. *J. Am. Chem. Soc.* **124,** 11270–11271 (2002).
33. Krogan, N. J. *et al.* Global landscape of protein complexes in the yeast *Saccharomyces cerevisiae*. *Nature* **440,** 637–643 (2006).
34. Gavin, A.-C. *et al.* Proteome survey reveals modularity of the yeast cell machinery. *Nature* **440,** 631–636 (2006).
35. Collins, S. R. *et al.* Toward a comprehensive atlas of the physical interactome of *Saccharomyces cerevisiae. Mol. Cell. Proteomics* **6,** 439–450 (2007).
36. Proudfoot, M. *et al.* Biochemical and structural characterization of a novel family of cystathionine β-synthase domain proteins fused to a Zn ribbon-like domain. *J. Mol. Biol.* **375,** 301–315 (2008).
37. Johnson, D. C., Dean, D. R., Smith, A. D. & Johnson, M. K. Structure, function, and formation of biological iron-sulfur clusters. *Annu. Rev. Biochem.* **74,** 247–281 (2005).
38. Lill, R. & Muhlenhoff, U. Maturation of iron-sulfur proteins in eukaryotes: mechanisms, connected processes, and diseases. *Annu. Rev. Biochem.* **77,** 669–700 (2008).

Supplementary Information is linked to the online version of the paper at www.nature.com/nature.

Acknowledgements We thank L. Kinsland for assistance with manuscript preparation, the Dreyfus Foundation for a New Faculty Award to H.L., NIH/NIGMS R01GM088276 to H.L. and S.E.E., and NIH/NCRR P41-RR016292 for the ACERT Center Grant to J.F. This work is based upon research conducted at the Advanced Photon Source (APS), Argonne National Laboratory, on the Northeastern Collaborative Access Team beamlines, which are supported by award RR-15301 from the US National Center for Research Resources at the US National Institutes of Health. Use of the APS is supported by the US Department of Energy, Office of Basic Energy Sciences, under contract no. DE-AC02-06CH11357.

Author Contributions Y.Z. determined the crystal structure of iron-free PhDph2, X.Z. performed the biochemical studies and prepared protein samples for spectroscopic and structural studies, A.T.T. determined the crystal structure of anaerobically purified PhDph2, M.L. and C.K. performed the Mössbauer spectroscopy, B.D. and J.F. performed the EPR spectroscopy, R.M.K. prepared the initial PhDph2 crystals, E.W. prepared the PhEF2 mutant proteins, S.E.E. supervised the crystallographic studies, H.L. supervised the biochemical studies and H.L., S.E.E. and C.K. prepared the manuscript.

Author Information Atomic coordinates and structure factors for the crystal structures reported here have been deposited with the Protein Data Bank under accession codes 3LZC for iron-free PhDph2 and 3LZD for reconstituted PhDph2. Reprints and permissions information is available at www.nature.com/reprints. The authors declare no competing financial interests. Readers are welcome to comment on the online version of this article at www.nature.com/nature. Correspondence and requests for materials should be addressed to H.L. (hl379@cornell.edu) or S.E.E. (see3@cornell.edu).

METHODS

Cloning, expression and purification of PhDph2 under anaerobic conditions. The gene encoding *P. horikoshii* Dph2 was amplified by PCR from *P. horikoshii* genomic DNA and inserted into pENTR/TEV/D-TOPO entry vector (Invitrogen), followed by recombination with pDESTF1 destination vector to create expression clones with an amino-terminal His_6 tag. The plasmids were transformed into the *E. coli* expression strain BL21(DE3) with pRARE. The cells were grown in lysogeny broth medium with 100 μg ml^{-1} ampicillin at 37 °C and were supplemented with $FeCl_3$, $Fe(NH_4)_2(SO_4)_2$ and L-cysteine to final concentrations of 50 μM, 50 μM and 400 μM, respectively, when the attenuance of the cell culture reached $D_{600\,nm}$ 0.8. The cells were induced at $D_{600\,nm}$ 0.8–1.0 with 0.1 mM isopropyl-β-D-thiogalactopyranoside (IPTG), at which point the culture flasks were sealed to limit the amount of oxygen in the system. The induced cells were incubated in a shaker (New Brunswick Scientific Excella E25) at 37 °C and 200 r.p.m. for 3 h before being transferred to the cold room at 4 °C, where they were kept overnight without agitation. Cells were collected on the second day by centrifugation at 6,371*g* (Beckman Coulter Avanti J-E), 4 °C for 10 min. Purification of PhDph2 was performed in an anaerobic chamber (Coy Laboratory Products) except for the centrifugation step. Cell pellets (from 2 l lysogeny broth culture) were resuspended in 30 mL lysis buffer (500 mM NaCl, 10 mM $MgCl_2$, 5 mM imidazole, 1 mM DTT and 20 mM Tris-HCl at pH 7.4). Cells were lysed by incubation with 0.3% (w/v) lysozyme (Fisher) at 26 °C for 1 h, followed by freezing in liquid nitrogen and thawing at 26 °C once. Cell debris was removed by centrifugation at 48,384*g* (Beckman Coulter Avanti J-E) for 30 min. The supernatant was incubated for 1 h with 1.2 ml Ni-NTA resin (Invitrogen) pre-equilibrated with the lysis buffer. The resin after incubation was loaded onto a polypropylene column and washed with 20 ml lysis buffer. PhDph2 was eluted from the column with elution buffers (100 mM or 150 mM imidazole in the lysis buffer, 3 ml each). The brown-coloured elution fractions were buffer-exchanged to 150 mM NaCl, 1 mM DTT and 200 mM Tris-HCl at pH 7.4 using a Bio-Rad 10-DG desalting column. The protein was further purified by heating at 95 °C for 10 min and centrifugation at 48,384*g* to remove the precipitate. Purified PhDph2 was concentrated using Amicon Ultra-4 centrifugal filter devices (Millipore).

Expression and purification of SeMet-substituted PhDph2. PhDph2.pDESTF1 was transformed into methionine-auxotrophic *E. coli* strain B834(DE3) pRARE that was obtained by transforming pRARE plasmid into B834(DE3). Cells were grown in M9 minimal medium supplemented with all amino acids (0.04 mg ml^{-1}) except L-methionine, 50 mg l^{-1} L-SeMet, ×1 MEM vitamin solution, 0.4% (w/v) glucose, 2 mM $MgSO_4$, 25 mg ml^{-1} $FeSO_4$ and 0.1 mM $CaCl_2$. The SeMet-substituted PhDph2 was overexpressed and purified as described above, except aerobically and no additional iron and cysteine were added to the media.

Expression and purification of ^{57}Fe-labelled PhDph2 for Mössbauer spectroscopy. *E. coli* BL21 pRARE cells transformed with PhDph2.pDESTF1 were grown in M9 minimal medium supplemented with 0.2% (w/v) glucose, 2 mM $MgSO_4$ and 0.1 mM $CaCl_2$ at 37 °C. The ^{57}Fe stock solution was prepared by dissolving ^{57}Fe powder (Isoflex USA) in HCl to final concentrations of 1 M iron and 2.5 M chloride. The ^{57}Fe stock solution and L-cysteine were added to M9 media to final concentrations of 100 μM and 400 μM, respectively, before induction. The cells were induced at $D_{600\,nm}$ 0.8 with 100 μM IPTG and incubated at 20 °C for an additional 20 h. ^{57}Fe-labelled PhDph2 was anaerobically purified by following the procedure used for the native protein purification. The final protein concentration, determined by Bradford protein assay (Bio-Rad), was 30 mg ml^{-1} (~800 μM). Iron was quantified by using the commercial DIFE-250 Quantichrom Iron Assay Kit (Bioassay Systems).

Cloning, expression and purification of PhEF2. Cloning of PhEF2 followed the same protocol as that of PhDph2. The plasmid was transformed into the *E. coli* expression strain BL21(DE3) with a pRARE plasmid. The cells were grown in lysogeny broth medium at 37 °C and induced at $D_{600\,nm}$ 1.0 with 0.1 mM IPTG. Cells were harvested after 3 h of induction by centrifugation at 6,371*g* (Beckman Coulter Avanti J-E) for 10 min. PhEF2 was purified through Ni-NTA affinity chromatography following the same protocol as for PhDph2. The protein was further purified by heating at 95 °C for 10 min and subsequent purification by fast protein liquid chromatography using a Superdex 200 gel filtration column and a Q6 anion exchange column (Bio-Rad).

Anaerobic reconstitution of PhDph2 activity and mass characterization of PhEF2. The reaction components, 12 μM PhEF2, 24 μM PhDph2 and 10 mM dithionite were added to 150 mM NaCl, 1 mM DTT and 200 mM Tris-HCl at pH 7.4 to a final volume of 15 μl in the anaerobic chamber under strictly anaerobic conditions. The reaction vials were sealed before being taken out of the anaerobic chamber. ^{14}C-SAM (2 μl, final concentration of 267 μM) was injected into each reaction vial to start the reaction. The reaction mixtures were vortexed briefly to mix and incubated at 65 °C for 40 min. The reaction was stopped by adding protein loading dye to the reaction mixture and subsequently heating at 100 °C for 10 min, followed by 12% SDS–polyacrylamide gel electrophoresis. The dried gel was exposed to a PhosphorImaging screen (GE Healthcare) and the radioactivity was detected using a STORM 860 PhosphorImager (GE Healthcare).

Enzymatic reactions with normal SAM followed the same procedure, except that normal SAM was introduced in the anaerobic chamber. The PhEF2 band from the Coomassie-blue-stained SDS–polyacrylamide gel was cut out and digested using trypsin. Digestion products were extracted and cleaned using a Millipore ZipTip C4, and then characterized by matrix-assisted laser desorption/ionization mass spectrometry at the Proteomics and Mass Spectrometry Core Facility of Cornell University.

Analysis of reaction products with high-performance liquid chromatography. Under anaerobic conditions, reactions were set up that contained 30 μM PhEF2, 30 μM PhDph2, 10 mM dithionite, 31 μM SAM, 150 mM NaCl, 1 mM DTT and 200 mM Tris-HCl at pH 7.4 in a final volume of 64 μl. The mixture was incubated at 65 °C for 5 min and then frozen at −20 °C. The reaction mixture was ice-thawed and TFA was added to a final concentration of 5%; this was followed by centrifugation to separate the precipitated proteins and the supernatant. The precipitated proteins were redissolved and PhEF2 was checked by matrix-assisted laser desorption/ionization mass spectrometry as described above to make sure the reaction had occurred. The supernatant was analysed by high-performance liquid chromatography (Shimadzu) on a C18 column (HαSprite) monitored at 260-nm absorbance, using a linear gradient from 0 to 40% buffer B over 20 min at a flow rate of 0.3 ml min^{-1} (buffer A: 50 mM ammonium acetate, pH 5.4; buffer B, 50% (v/v) methanol/water).

^{1}H NMR of reaction mixture. A complete reaction (260 μM PhDph2, 10 mM dithionite and 1,000 μM SAM, in 1 ml of 100 mM phosphate buffer with 150 mM sodium chloride, pH 7.4) and a control (without PhDph2 or without dithionite) were set up anaerobically. After incubation at 65 °C for 40 min, PhDPh2 was removed using a Millipore Microcon YM-10 filter unit. The flow-through was lyophilized overnight to dryness and then dissolved in 300 μl D_2O for NMR. A Shigemi D_2O-matched NMR tube was used. ^{1}H NMR spectra were obtained on an INOVA 400 spectrometer. In comparison with controls, four new peaks were identified by ^{1}H NMR: (a) 0.95 p.p.m. (t, 1H, $J = 7.6$ Hz), (b) 1.88 p.p.m. (m, 1H), (c) 2.12 p.p.m. (m, 2H) and (d) 2.43 ppm (t, 1H, $J = 7.5$ Hz). A H-H DQCOSY two-dimensional NMR spectrum (data not shown) showed that peak (a) is coupled to peak (b) and that peak (c) is coupled to peak (d) and another peak (3.78 p.p.m.) that is hidden under the huge signal from buffer. NMR data were analysed using MESTRENOVA (version 6.0.1).

Dansylation reaction to detect the mass spectrum of the reaction products by LC–MS. NMR samples were desalted and purified by thin-layer chromatography silica gel 60 F254 (EMD Chemicals) with developing solvent (*n*-butanol/acetic acid/water, 2:1:1). The desired product bands (retention factor (R_f) 0.15–0.65, which is less than the R_f value of 5′-deoxy-5′-methylthioadenosine) were cut off the thin-layer chromatography plates and the products were washed off the silica gel using water and lyophilized overnight to dryness. The lyophilized products were dissolved with 50 mM sodium bicarbonate to a final concentration approximately five times of that of the NMR reaction. The solution was adjusted to pH 9–10 using 12% NaOH. Dansylation reactions were initiated by adding half the volume of 50 mM dansyl chloride in acetonitrile to the solution, and the reactions were carried out at room temperature (25 °C) in the dark for 30 min. Dansylated products were separated and analysed by LC–MS with a linear gradient from 0 to 80% solvent B over 33 min at a flow rate of 0.8 ml min^{-1}. LC–MS experiments were carried out on a Shimadzu LCMS QP8000α with a C18 column (250 mm × 4.6 mm, 10 μm, Grace Davison Discovery Sciences) monitoring at 254 and 335 nm using positive mode for mass detection. Solvents for LC–MS were water with 0.1% formic acid (solvent A) and acetonitrile with 0.1% formic acid (solvent B).

Sample preparation for Mössbauer spectroscopy and EPR. Anaerobically purified, ^{57}Fe-labelled PhDph2 was dialysed into a buffer containing 200 mM Tris-HCl (pH 7.4), 150 mM NaCl, 1 mM DTT and 10% glycerol, and concentrated to 25–30 mg ml^{-1}. The sample was frozen in liquid nitrogen in the anaerobic chamber for Mössbauer spectroscopy. For EPR measurements, PhDph2 (700 μM, with 15% glycerol) with and without 16 mM dithionite was incubated for 30 min before loading into an EPR quartz tube in the glovebox.

Crystallization and structure determination of iron-free PhDph2. Aerobically purified, iron-free PhDph2 proteins were dialysed into 10 mM sodium acetate at pH 4.6 and concentrated to 12 mg ml^{-1} for the crystallization experiments. The native protein was subjected to a series of sparse matrix screens (Hampton Research, Emerald Biostructures) using the hanging-drop vapour-diffusion method at 18 °C to determine initial crystallization conditions. The best crystals for both SeMet-substituted and native PhDph2 were obtained from 6–8% PEG 4000, 0.1 M ammonium acetate, 0.2 M KCl, 2% ethylene glycol and 0.05 M sodium citrate at pH 5.1–5.3. These crystals belong to the space group $P2_12_12_1$ and have typical unit-cell dimensions of $a = 58.5$ Å, $b = 82.0$ Å and $c = 160.0$ Å.

Each asymmetric unit contains two monomers, corresponding to a solvent content of 50.3% and a Matthews coefficient of 2.47 $Å^3\,Da^{-1}$.

The PhDph2 SeMet crystals were briefly transferred into a solution containing 6% glycerol, 16% ethylene glycol, 10% PEG 4000, 0.2 M ammonium acetate, 0.2 M KCl and 0.1 M sodium citrate at pH 5.3 for cryoprotection. The crystals were allowed to soak in the cryo-solution for 30–45 s before being plunged into liquid nitrogen. In an attempt to reconstitute the iron–sulphur clusters in crystals, native crystals were soaked in 10% PEG 4000, 100 mM citrate (pH 5.3), 200 mM ammonium acetate, 200 mM KCl, 10% ethylene glycol, 8 mM SAM, 4 mM $Fe(NH_4)_2(SO_4)_2$, 4 mM NaS and 40 mM DTT for 1 h before undergoing the same cryoprotection and freezing procedure described above.

Data sets were collected at the Advanced Photon Source beamlines 24-ID-C and 24-ID-E using ADSC Quantum 315 CCD detectors. For the single-wavelength SeMet data set, the energy was selected to maximize $\Delta f''$ of the incorporated selenium (12,661.5 eV, 0.97922 Å). Data sets were integrated and scaled using HKL2000[39]. Data-processing statistics are summarized in Supplementary Table 1.

Eight selenium atom positions were determined using HKL2MAP[40]. These sites were used for single-wavelength anomalous diffraction phasing using MLPHARE[41] at 2.5 Å resolution. Initial phases were further improved through density modification, twofold non-crystallographic symmetry averaging and phase extension for the 2.3 Å resolution native data using RESOLVE[42,43]. The resulting map was readily interpretable and an initial model was built using the interactive graphics program COOT[44]. Model refinement was carried out through alternating cycles of manually rebuilding using COOT, restrained refinement and water-picking using REFMAC5[45] and PHENIX[46]. Structure-refinement statistics are summarized in Supplementary Table 1.

Crystallization and structure determination of reconstituted PhDph2. Reconstituted PhDph2 protein was dialysed into 100 mM NaCl, 1 mM DTT and 10 mM sodium acetate at pH 4.6, concentrated to 20 mg ml^{-1} and crystallized anaerobically at 26 °C in the glovebox using the hanging-drop vapour-diffusion method. Anoxic sparse matrix screening solutions (Hampton Research, Emerald Biostructures) were used for initial crystallization screens. The optimized crystallization condition is as follows: drops were set up with 1.3 µl protein and an equal volume of 25–30% PEG 400, 0.2 M lithium sulphate and 0.1 M MES at pH 6.5, and were equilibrated against a reservoir solution of 0.6 M lithium chloride. Crystals appeared in a week and belonged to the same space group as that of the iron-free structure ($P2_12_12_1$, with average unit-cell dimensions of $a = 55.7$ Å, $b = 80.5$ Å and $c = 162.1$ Å). Before the data collection experiment, crystals were cryoprotected with 2.5–5% ethylene glycol, 25–30% PEG 400, 0.2 M lithium sulphate and 0.1 M MES at pH 6.5 and then plunged directly into liquid nitrogen in the glovebox. A total of 200° of data were recorded at an energy of 12,662.0 eV on an ADSC Quantum 315 CCD detector. The data were integrated and scaled to 2.1 Å resolution using HKL2000[39]. The previously solved structure of PhDph2 lacking the iron–sulphur cluster was used to generate phases by Fourier synthesis. A difference Fourier map was calculated and averaged for the two monomers to improve the electron density, and the resulting map was used to model the [4Fe–4S] cluster. A 2.8 Å resolution anomalous difference Fourier map calculated from a data set collected at 7,150 eV (1.73405 Å) was also used as a reference for positioning the [4Fe–4S] cluster (not shown). The structure was refined using CNS[47]. X-ray experiment and structure-refinement statistics are summarized in Supplementary Table 1.

Ultraviolet–visible spectroscopy. Samples of PhDph2 (50 µM), with and without dithionite, were prepared anaerobically in 150 mM NaCl and 200 mM Tris-HCl at pH 7.4. The sample treated with dithionite was allowed to incubate for 30 min after adding the reducing agent at a final concentration of 0.5 mM. The samples were sealed in a quartz cell (100 µl each) before being taken out of the anaerobic chamber. Ultraviolet–visible spectra were obtained on a Cary 50 Bio UV-Vis spectrophotometer (Varian), scanning from 200 nm to 800 nm. The baseline was corrected with the buffer used to prepare the samples.

EPR spectroscopy. ESR spectra were recorded at ACERT on a Bruker EMX spectrometer at a frequency of 9.24 GHz under standard conditions in quartz tubes with internal diameters of 4 mm. The tubes were filled with PhDph2 solutions in an oxygen-free atmosphere and sealed under vacuum at 77 K. ESR measurements at 5–50 K were carried out using an ESR 10 liquid-helium cryostat (Oxford Instruments). The spectrometer settings were as follows: modulation frequency, 100 kHz; modulation amplitude, 8 G; microwave power, 0.63 mW.

Mössbauer spectroscopy. Mössbauer spectra were recorded on a spectrometer from WEB Research operating in the constant-acceleration mode in transmission geometry. Spectra were recorded with the temperature of the sample maintained at 4.2 K using a Janis SVT-400 cryostat in an externally applied magnetic field of 53 mT oriented parallel to the γ-beam. The quoted isomer shifts are relative to the centroid of the spectrum of a foil of α-Fe metal at room temperature. Data analysis was performed using the program WMOSS from WEB Research.

39. Otwinowski, Z. & Minor, W. Processing of X-ray diffraction data collected in oscillation mode. *Methods Enzymol.* **276**, 307–326 (1997).
40. Sheldrick, G. M. A short history of SHELX. *Acta Crystallogr. A* **64**, 112–122 (2008).
41. Collaborative. Computation Project, Number 4. The CCP4 suite: programs for protein crystallography. *Acta Crystallogr. D* **50**, 760–763 (1994).
42. Terwilliger, T. C. Reciprocal-space solvent flattening. *Acta Crystallogr. D* **55**, 1863–1871 (1999).
43. Terwilliger, T. C. Maximum-likelihood density modification. *Acta Crystallogr. D* **56**, 965–972 (2000).
44. Emsley, P. & Cowtan, K. Coot: model-building tools for molecular graphics. *Acta Crystallogr. D* **60**, 2126–2132 (2004).
45. Murshudov, G. N., Vagin, A. A. & Dodson, E. J. Refinement of macromolecular structures by the maximum-likelihood method. *Acta Crystallogr. D* **53**, 240–255 (1997).
46. Adams, P. D. *et al.* PHENIX: building new software for automated crystallographic structure determination. *Acta Crystallogr. D* **58**, 1948–1954 (2002).
47. Brünger, A. T. *et al.* Crystallography & NMR system: a new software suite for macromolecular structure determination. *Acta Crystallogr. D* **54**, 905–921 (1998).

Author Queries

Journal: **Nature**
Paper: **nature09138**
Title: **Diphthamide biosynthesis requires an organic radical generated by an iron–sulphur enzyme**

Query Reference	Query
1	AUTHOR: When you receive the PDF proofs, please check that the display items are as follows (doi:10.1038/nature09138): Figs 1, 6 (black & white), 2–5 (colour). Please check all figures very carefully as they have been re-labelled, re-sized and adjusted to Nature's style. Please check the title and the first paragraph with care, as they may have been re-written to aid accessibility for non-specialist readers.
2	PROOFREADER: Please update/confirm the tentative publication date.
3	AUTHOR: is the magnification number (1.00) correct for dansyl ABA in the lowest plot?

For Nature office use only:

Layout	☐	Figures/Tables/Boxes	☐	References	☐
DOI	☐	Error bars	☐	Supp info (if applicable)	☐
Title	☐	Colour	☐	Acknowledgements	☐
Authors	☐	Text	☐	Author contribs (if applicable)	☐
Addresses	☐	Methods (if applicable)	☐	COI	☐
First para	☐	Received/Accepted	☐	Correspondence	☐
Display items	☐	AOP (if applicable)	☐	Author corrx	☐